ACSNANO

www.acsnano.org

ARTICLE

Radiolabeled Biodistribution of Expansile Nanoparticles: Intraperitoneal Administration Results in Tumor Specific Accumulation

Aaron H. Colby,* Jack Kirsch, Amit N. Patwa, Rong Liu, Beth Hollister, William McCulloch, Joanna E. Burdette, Cedric J. Pearce, Nicholas H. Oberliels, Yolonda L. Colson, Kebin Liu, and Mark W. Grinstaff

Cite This: https://doi.org/10.1021/acsnano.2c08451

Read Online

ACCESS | Metrics & More | Article Recommendations | Supporting Information

ABSTRACT: **Nanoparticle biodistribution *in vivo* is an essential component to the success of nanoparticle-based drug delivery systems. Previous studies with fluorescently labeled expansile nanoparticles, or "eNPs", demonstrated a high specificity of eNPs to tumors that is achieved through a materials-based targeting strategy. However, fluorescent labeling techniques are primarily qualitative in nature and the gold-standard for quantitative evaluation of biodistribution is through radiolabeling. In this manuscript, we synthesize ^{14}C-labeled eNPs to quantitatively evaluate the biodistribution of these particles in a murine model of intraperitoneal mesothelioma via liquid scintillation counting. The results demonstrate a strong specificity of eNPs for tumors that lasts one to 2 weeks postinjection with an overall delivery efficiency to the tumor tissue of 30% of the injected dose which is congruent with prior reports of preclinical efficacy of the technology. Importantly, the route of administration is essential to the eNP's material-based targeting strategy with intraperitoneal administration leading to tumoral accumulation while, in contrast, intravenous administration leads to rapid clearance via the reticuloendothelial system and low tumoral accumulation. A comparison against nanoparticle delivery systems published over the past decade shows that the 30% tumoral delivery efficiency of the eNP is significantly higher than the 0.7% median delivery efficiency of other systems with sufficient quantitative data to define this metric. These results lay a foundation for targeting intraperitoneal tumors and encourage efforts to explore alternative, nonintravenous routes, of delivery to accelerate the translation of nanoparticle therapies to the clinic.**

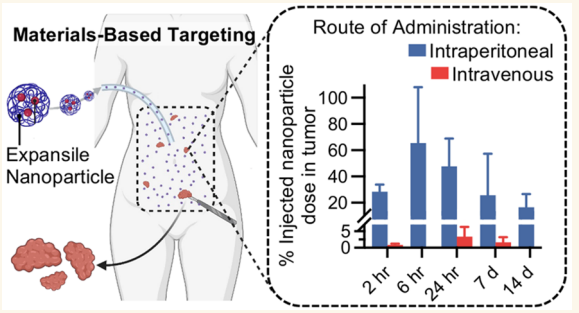

KEYWORDS: *Radiolabeled biodistribution, expansile nanoparticle, liquid scintillation counting, intraperitoneal administration, materials-based targeting*

INTRODUCTION

Tumor-specific delivery of therapeutic agents has proven to be an elusive goal in the field of nanoparticle-based drug delivery systems. Despite early enthusiasm for nanoparticle-based drug delivery technologies at the turn of the millennium, the paucity of successful commercialization stories to date is evidence of the stark reality that the vast majority of these systems have failed the combined tests of translation and commercialization. While Abraxane has achieved enduring clinical success and is oft-described as one of the earliest FDA-approved nanoparticles for the treatment of cancer, its simple paclitaxel-albumin complexes are hardly representative of the myriad complex polymer- or inorganic core-based nanoparticle designs under investigation. Furthermore, while other "nano" formulations, such as Doxil (1995), Marqibo (2012), ONIVYDE (2015) and Vyxeox (2017) are FDA-approved, these are all liposomal nano formulations, as opposed to solid nanoparticles and, as such, are representative of liposomal, rather than nanoparticle, success. In fact, polymer nanoparticles have yet to achieve commercial success with multiple technologies being discontinued following poor clinical trial results, including, among others: Paclimer (biodegradable paclitaxel microspheres),[1] discontinued after Phase I clinical trials; and, PG-

Received: August 23, 2022
Accepted: January 23, 2023

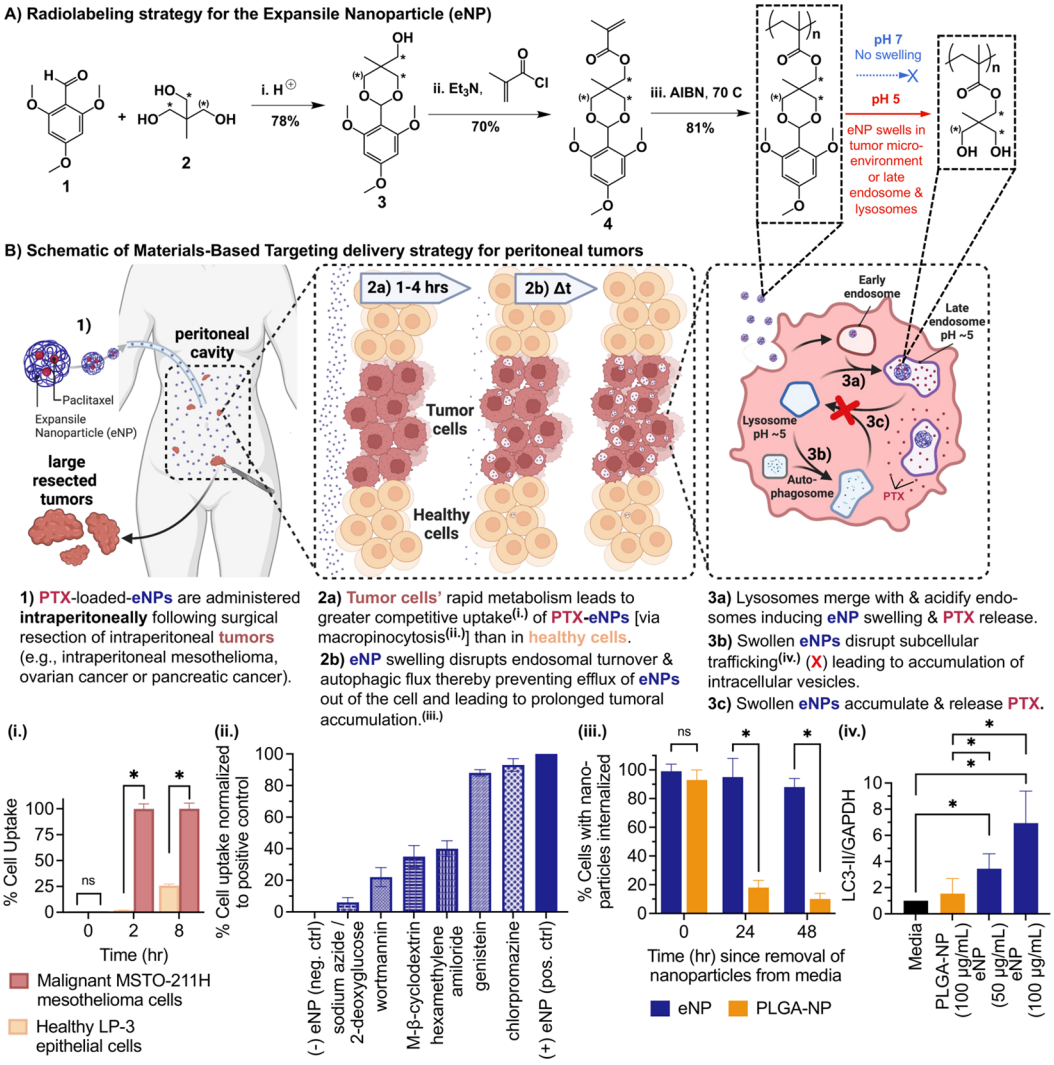

Figure 1. Radiolabeling strategy and delivery concept for the Expansile Nanoparticle "eNP" technology. A) The eNP is radiolabeled with two ^{14}C isotopes per monomer unit (denoted by *) to provide traceability of the particle. B) Schematic depiction of the Materials-Based Targeting delivery strategy which leverages intraperitoneal administration in patients with peritoneal cancers. This working hypothesis is supported by i.) faster uptake of particles in malignant vs healthy cells *in vitro*; ii.) cellular internalization through macropinocytosis *in vitro*; iii.) prolonged retention of eNPs within mesothelioma cells *in vitro* after removal of the source of particles, which is in contrast to poly(lactic-*co*-glycolic) acid (PLGA) nanoparticles that are rapidly excreted from cells; and, iv.) disruption of subcellular trafficking by eNPs leading to accumulation of autophagic substrates (i.e., LC3-II) and, subsequently, prolonged cellular retention. Data in subpanels i.) and iv.) reproduced with permission from ref 12. Copyright 2016 Elsevier. Data in subpanel ii.) reproduced with permission from ref 30. Copyright 2013 American Chemical Society.

TXL [poly(L-glutamic acid)-paclitaxel],[2] discontinued after Phase III clinical trials. Perhaps most disappointing was the bankruptcy of BIND Therapeutics in 2016 following poor clinical trial results of its lead cancer drug, BIND-014. Notwithstanding a wealth of diversity in particle design, of the thousands of nanoparticle technologies published in the last two decades, one common link shared by nearly all systems is a reliance upon one of two basic strategies to target tumors: "passive targeting", or "active targeting". Passive targeting aims to leverage the enhanced permeability and retention (EPR) effect—a phenomenon describing tumoral accumulation of intravenously administered nanoparticles as a result of the highly fenestrated or "leaky" vasculature found in large (>1 cm^3) tumors.[3] However, the translatability of the EPR effect is questioned by many researchers and even its proponents agree that heterogeneity among patient tumors is greater than in animal models making clinical translation of pre-clinical outcomes less certain.[4] Active targeting aims to decorate the surface of nanoparticles with antibodies whose receptors are overexpressed on the surface of cancer cells thereby encouraging tumoral sequestration following intravenous administration. However, the need to tailor an antibody to one cancer subtype overexpressing a particular receptor reduces the flexibility of a given system, even if successfully developed.[3,5,6] Further, the acquisition of resistance, immunogenicity and the tendency of cancers to alter surface markers over time, as well as during treatment, rapidly leads to obsolescence of specific antibodies, often within one to two years.[7,8] As such, neither passive nor active tumor targeting have yielded significant success.

In a reflection of this, in 2016, Wilhelm et al. published a thorough review of the effectiveness of past and current nanoparticle delivery systems in localizing to tumors.[9] The authors performed a systematic search of the published

https://doi.org/10.1021/acsnano.2c08451
ACS Nano XXXX, XXX, XXX−XXX

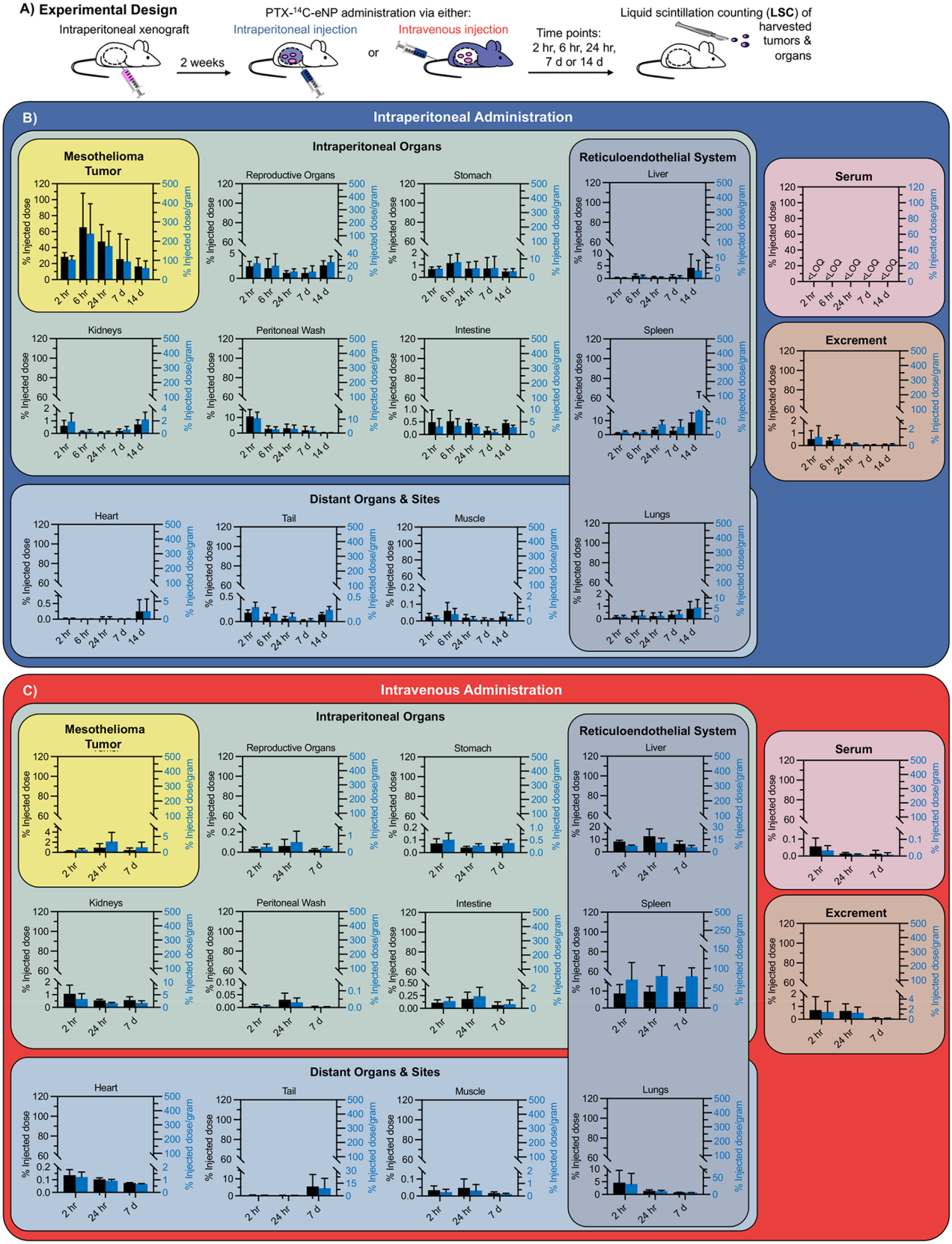

Figure 2. A) Experimental design for the biodistribution study of PTX-^{14}C-eNPs in tumor bearing animals. Quantification of radioactivity and corresponding % injected dose as well as % injected dose per gram of tissue are plotted for major organs following B) intraperitoneal and C) intravenous administration of PTX-^{14}C-eNPs. Data are presented with uniform *y*-axis maxima on all plots to facilitate visual comparison across panels. For readers preferring to see individually scaled axes, please refer to SI Figure 6.

https://doi.org/10.1021/acsnano.2c08451
ACS Nano XXXX, XXX, XXX−XXX

literature to find all nanoparticle publications with quantitative biodistribution data that reported the percent injected dose (% ID) or %ID/gram in the tumor for at least three different time points. Of the >40,000 "nanoparticle delivery" papers, 117 met the requirements for quantitative analysis by the authors. The median delivery efficiency, defined as the sum of the area under the curve (AUC) of the concentration vs time graph normalized by the tissue mass and study duration, was found to be a meager 0.7%. Wilhelm et al. argue that this paltry delivery efficiency is reflective of the need for alternative approaches to nanoparticle delivery that leverage mechanisms other than traditional active or passive targeting, and we concur with this assessment.

In this manuscript, we quantitatively evaluate the biodistribution of paclitaxel-loaded expansile nanoparticles (PTX-eNPs) through incorporation of a ^{14}C-label into the eNP polymer. Previously published studies using fluorescently labeled eNPs to qualitatively assess biodistribution demonstrated specificity for tumors in multiple disease models (e.g., intraperitoneal mesothelioma, ovarian and pancreatic cancers).[10−15] In one study, rhodamine-labeled eNPs were found to accumulate in and identify pancreatic tumors with a specificity of 99% and an accuracy of 92% as determined by visual inspection of the rhodamine distribution.[13] The mechanism responsible for eNP tumor-targeting, which is described in Liu et al., 2016[12] and Colby et al., 2017,[16] is different from other systems and stands apart from traditional passive and active targeting techniques. In brief, eNPs employ a Materials-Based Targeting strategy which leverages fundamental pathophysiological properties of tumors (e.g., mildly acidic extracellular environment and high metabolic rate), which are fundamental Hallmarks of Cancer,[17,18] as well as disruption of autophagy,[12] to achieve rapid internalization and prolonged retention within tumors (Figure 1B). Further discussion of this mechanism follows in the results and discussion section, below. Integral to this process is the route of administration. eNPs are designed to be administered intraperitoneally, rather than intravenously, and are best suited for treating intraperitoneal cancers (e.g., ovarian cancer,[19,20] pancreatic cancer,[11,13] or intraperitoneal mesothelioma[12,14−16,21,22]). In this manner, eNPs leverage the inherent proximity and direct surface contact to tumors afforded by intraperitoneal administration. Because of the advantage provided by target proximity, intraperitoneal administration is often used for delivery of traditional chemotherapeutics, such as paclitaxel or cisplatin, to patients with peritoneal carcinomatosis (i.e., tumors disseminated across the mucosal linings and surfaces of the vital organs in the peritoneum).[23−27] However, it has been infrequently explored as an administration method for potentiation of nanoparticle therapeutics. Herein, we report on: the synthesis of paclitaxel-loaded ^{14}C-labeled eNPs (PTX-^{14}C-eNPs); the quantitative biodistribution of these particles when administered intraperitoneally and, for comparison, intravenously; and, a comparison of eNP tumor specificity versus other published nanoparticle systems.

RESULTS AND DISCUSSION

Synthesis of "hot" ^{14}C-eNP Monomer. From the perspective of traceability, the preferred location to introduce a ^{14}C label to the eNP monomer is the methacrylic acid functionality. However, from a manufacturability standpoint, this is impractical as placement of the ^{14}C in such close proximity to the reactive alkene group would lead to premature polymerization. Alternatively, labeling of the methoxy functionalities on the 2,4,6-trimethoxybenzaldehyde protecting group is an obvious location to incorporate a label; however, due to the rapid hydrolysis of this protecting group once the eNP reaches its target, it is an unsuitable handle from which to track the distribution of the particles. Therefore, we chose to label the 1,1,1-tris(hydroxymethyl) ethane functionality that links the methacrylic acid to the hydrolyzable protecting group (Figure 1A). Beginning with commercially available ^{14}C-formaladehyde, we performed a three step synthesis in which: 1) ^{14}C-formaldehyde was reacted with propionaldehyde to generate "hot" 1,1,1-tris(hydroxymethyl)ethane (Figure 1A, 2); 2) this "hot" intermediate was reacted with 2,4,6-trimethoxybenzaldehyde (Figure 1A, 1) to produce "hot" (5-methyl-2-(2,4,6-trimethoxyphenyl)-1,3-dioxan-5-yl)methanol (Figure 1A, 3); and, 3) this hot intermediate was reacted with

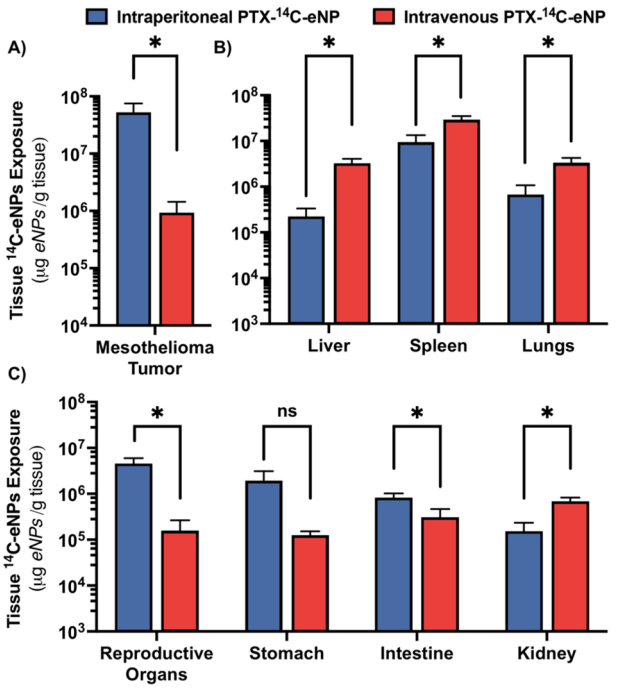

Figure 3. Comparison of total tissue exposure to eNPs by administration route. Tissue exposure calculated as $AUC_{0-168\ h}$ for the A) mesothelioma tumor, B) organs of the reticuloendothelial system and C) intraperitoneal organs. Exposure is displayed in μg eNP per g of tissue. * = $p < 0.05$.

methacryloyl chloride to produce the "hot" ^{14}C-eNP monomer (Figure 1A, 4). The monomer structure was confirmed, and compared to cold eNP monomer via NMR and mass spectrometry (SI Figure 1). The radiochemical purity of the ^{14}C-eNP monomer is 97.6% by high-performance liquid chromatography (HPLC) (SI Figure 2) with a specific activity of 5 mCi/mmol as determined by mass spectrometry.

Synthesis of "hot" ^{14}C-eNP Polymer. We polymerized the ^{14}C-eNP monomer using AIBN according to previously published protocols[15] and obtained 14 mCi of polymer (81% yield) [Figure 1A, (iii)]. NMR spectroscopy confirmed the polymer structure (SI Figure 3A,B) and GPC analysis provided the molecular weight and radiochemical purity (38 kDa and >99.9%, respectively; SI Figure 3C−E), which confirmed no significant impact of the radiolabeling on the polymerization compared to "cold" syntheses.[15] The specific activity of the

https://doi.org/10.1021/acsnano.2c08451
ACS Nano XXXX, XXX, XXX−XXX

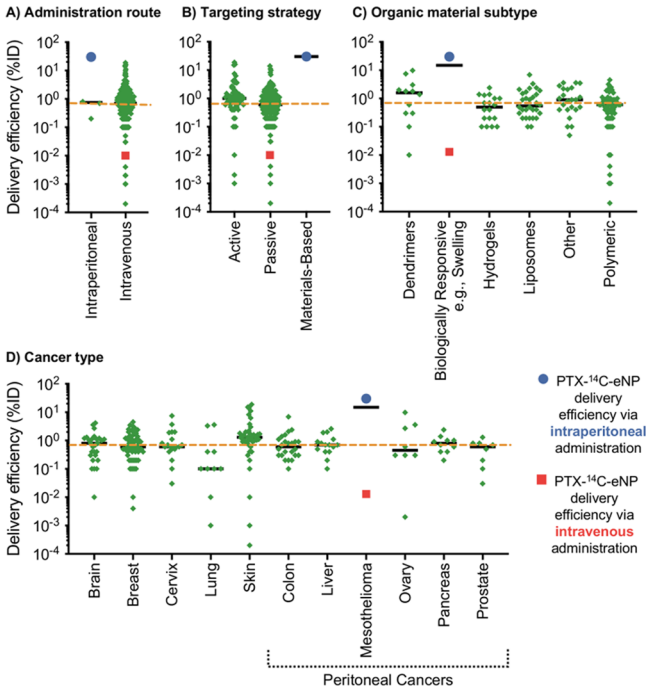

Figure 4. Comparison of PTX-^{14}C-eNP delivery efficiency against published nanoparticle systems generated by Wilhelm et al. Delivery efficiency represents the normalized integral of the area under the curve on a tumor concentration vs. time plot (as in Figure 2). Historical data from Wilhelm et al. are plotted as green diamonds. Current data for delivery of PTX-^{14}C-eNPs (blue circles for intraperitoneal administration, red squares for intravenous administration), which are not contemporaneous with Wilhelm et al.'s data, are plotted next to these data to demonstrate the combined importance of: A) administration route, B) targeting strategy, C) organic material type, and D) cancer type to optimizing tumoral delivery. The median delivery efficiency for all technologies surveyed by Wilhelm et al. (0.7%ID) is represented by orange dashed lines. Individual category median values are represented by horizontal black lines. Data from Wilhelm et al. reprinted with permission from ref 9. Copyright 2016 Spring Nature.

polymer is 3.88 μCi/mg. To evaluate the stability of the ^{14}C-eNP polymer, we performed GPC analysis at two-weeks and four-weeks post synthesis. The results demonstrate no significant change in molecular weight or radiochemical purity indicating that, when stored at −20 °C, the ^{14}C-eNP polymer is stable for at least 4 weeks (SI Figure 4).

Synthesis of "hot" PTX-^{14}C-eNPs. We performed the synthesis of paclitaxel-loaded ^{14}C-eNPs (PTX-^{14}C-eNPs) using a scaled-down version of our recently developed and published procedure for pilot-scale production of PTX-eNPs.[15] We targeted a final activity of 8−10 μCi per 250 μL dose of PTX-^{14}C-eNPs (the dose for one animal) so that as little as 0.01% of the injected dose would be detectable [limit of detection (LOD) via liquid scintillation counting (LSC) for ^{14}C is 1 nCi/mL of extracted tissue (SI Figure 5)]. To achieve this target specific activity, we combined "hot" and "cold" eNP polymer in a 3:1 ratio with a resulting specific acitivity of 34.5 μCi/mL, or 8.6 μCi per 250 μL dose. We loaded the particles with the "standard" payload of 5% PTX,[16] yielding a final concentration of 1 mg/mL in the PTX-^{14}C-eNPs. The concentration of eNPs/mL as determined using tunable-resistive pulse sensing (i.e., "qNano" technology from iZon Ltd.) was 1×10^{12} particles/mL. Given radiolabeling of 34.5 μCi/mL, this translates to an average of 34.5 attoCuries/eNP. Particle diameter was found to be 54 nm with a polydispersity index of 0.1.

Selection of Tumor Model and Quantification Techniques. PTX-eNPs are efficacious in murine models of intraperitoneal mesothelioma.[12,15,16] We therefore selected this well-characterized and published model for the biodistribution study, wherein we administered PTX-^{14}C-eNPs 14 days after xenografting. We quantified radioisotope distribution via LSC of individual organs, tissues and fluids (three animals per group and time point). LSC is a traditional extraction-and-quantification method wherein the entirety of each organ or tissue is removed, homogenized and the tracer isotope quantified. LSC is a preferred method over quantitative whole-body autoradiography (QWBA) as it more accurately accounts for the majority of the injected dose of radioisotope on a per organ basis.

Biodistribution of PTX-^{14}C-eNPs in Intraperitoneal Mesothelioma. LSC analysis of organs and tissues from animals receiving intraperitoneal injections of PTX-^{14}C-eNPs reveals rapid and specific localization to tumor tissue (within 2−6 h) with prolonged retention for up to 2 weeks (Figure 2). Accumulation within the tumor reaches a maximum of 65% of the injected dose (%ID) 6 h after injection and persists with nearly 50%ID present after 24 h and 25%ID present after 1 week.[9] Furthermore, intraperitoneally administered PTX-^{14}C-eNPs avoid rapid uptake in, and clearance by, the spleen, liver and lungs—the three major organ components of the reticuloendothelial system (RES) responsible for clearing foreign colloids,[28,29] with accumulation of <5%ID at any point up to 1 week. This is, perhaps, not surprising as the filtration and colloidal scavenging functions of the RES organs are focused on the circulatory system, which is bypassed by intraperitoneal administration. Notwithstanding this, ~10%ID is present in the spleen 2 weeks post injection and this likely reflects the gradual hydrolysis of the eNP polymer leading to disintegration of the particle network and subsequent eventual clearance through the RES.

Of further note is that organs within the peritoneal cavity that experienced a similar duration and degree of exposure to the PTX-^{14}C-eNPs, including the kidneys, stomach, intestine and reproductive organs, also show minimal eNP accumulation (<2.5% of the injected dose at any time point). A wash of the peritoneal cavity at each time point recovers nearly 10%ID 2 h post administration but <2.5%ID at later time points. This is a reflection of the rapid (several hour timespan)[12,16] uptake of eNPs within the tumor. Distant sites, including the heart, tail and muscle from the thigh, showed negligable accumulation (<0.5%ID) at any time point. Similarly, PTX-^{14}C-eNP levels in the excrement are negligable and serum levels are below the limit of quantification (LOQ). Low levels in the serum are consistent with our prior *in vivo* studies that showed no significant weight loss or toxicity and histopathological analysis from this study (SI Figure 7) is consistent with these results.[10−12,14,16,19]

In contrast to the high tumoral accumulation resulting from intraperitoneal administration, following intravenous administration, PTX-^{14}C-eNPs do not substantially localize to tumors (<2%ID). Rather, accumulation was greatest in organs of the RES, in particular the spleen (Figure 2C). Figure 3 directly compares the area under the curve from adminstration to day seven (AUC) for intraperitoneal versus intravenous delivery

https://doi.org/10.1021/acsnano.2c08451
ACS Nano XXXX, XXX, XXX−XXX

routes. Intraperitoneal administration results in a >50-fold increase in PTX-^{14}C-eNPs accumulation within the tumor (Figure 3A) as well as a nearly 10-fold reduction in RES accumulation (Figure 3B). Particle accumulation in peritoneal organs is somewhat higher following intraperitoneal, as compared to intravenous, delivery with the exception of renal accumulation of PTX-^{14}C-eNPs. This is not surprising due to the direct contact between particles and organs (Figure 3C).

Materials-Based Targeting. We term the mechanism behind this tumor-specific localization and persistance "materials-based targeting". Figure 1B offers a visual description of our working hypothesis behind this mechanism. Briefly, differential uptake of eNPs occurs in tumoral versus healthy cells because the elevated metabolism of tumor cells compared to nontumoral cells leads to more rapid internalization of particles (Figure 1B, i.).[12] Particles are internalized via macropinocytosis thereby entering into the intracellular trafficking cycle (Figure 1B, ii.).[30] Following particle internalization, intraendosomal swelling of the hydrolyzable eNP polymer disrupts subcellular trafficking thereby leading to an accumulation of intracellular vessicles, including those endosomes that contain particles (Figure 1B, iv.).[12] As a result, eNPs accumulate intracellularly and persist within the cell. This is in contrast to nonswelling poly(lactic-*co*-glycolic) acid nanoparticles (PLGA-NPs) that, even though they are internalized to a similar extent as eNPs *in vitro*, are cleared rapidly from cells once the extracellular source of particles is removed (Figure 1B, iii.). Importantly, previous *in vivo* studies demonstrate that materials-based targeting is not common to all particles. Side-by-side comparisons of fluorescently labeled eNPs, PLGA-NPs, which are nonswelling, and poly(ethylene glycol) (PEG) coated-eNPs, which are not rapidly endocytosed as a result of the PEG coating, demonstrate gross tumoral accumulation of eNPs and no detectable accumulation of PLGA-NPs or PEGylated eNPs.[13] Here, we further demonstrate that route of administration is essential to materials-based targeting; when PTX-^{14}C-eNPs are injected intravenously, there is negligable accumulation in tumors with almost immediate first-pass clearance into the organs of the RES, in particular the spleen (Figures 2 and 3). This is consistent with decades of nano- and microparticle research dating back to the 1970s demonstrating that intravenous administration of colloids leads primarily to accumulation within the RES.[31−36] Materials-based targeting approaches, coupled with optimized adminstration routes, overcome this drug delivery barrier.

Comparison of ^{14}C-eNP Tumor Specificity to Other Nanoparticle Systems. In 2020, Chen et al. published a follow up to Wilhelm et al.'s 2016 study showing a median delivery efficiency of 0.7%ID of published nanoparticle systems reaching the target (i.e., tumor) tissue. In this more recent work, Chen et al. used physiologically based pharmacokinetic models to evaluate published nanoparticle biodistribution data from 2005 to 2018 and reports similar mean delivery efficiencies among 376 qualifying published data sets with 2.2%ID and 1.2%ID accumulating at the target 1 day and 7 days post injection, respectively.[37] The majority of nanoparticles localize primarily to organs of the RES and to the kidneys. These results are consitent with the recent report by Varani et al. in 2021 evaluating the biodistribution of a series of PLGA-NPs in nontumor bearing animals which shows that, despites variations in particle size and surface charge, intravenous administration leads to accumulation primarily in organs of the RES and the kidneys.[38] While these reviews offer a rather dim picture of the overall nanoparticle landscape, some encouraging studies are also present. For example, 35% of the injected dose of a core−shell silver/polymeric nanoparticle described by Farrag et al. in 2017, accumulates in the target tumor tissue 1 h post injection, though this decreases to 22%ID 4 h post injection and was not evaluated beyond these early time points.[39] More recently, in 2021, Wang et al. published a radiolabeled biodistribution study of RNA nanoparticles in which 5% of the injected dose reached the tumor.[40]

Our biodistribution data following intravenous administration of PTX-^{14}C-eNPs is congruent with this body of published literature. Following intravenous administration, in which only the EPR effect can be relied upon to preferentially direct PTX-^{14}C-eNP accumulation to tumors, a paltry 0.01%ID accumulates in the tumor with the majority accumulating in the RES. In contrast, following intraperitoneal administration, which leverages materials-based targeting,[12,16] a 3,000-fold increase in delivery efficiency of PTX-^{14}C-eNPs is achieved with 30%ID accumulating in the tumor. To facilitate comparison of these starkly contrasting results and also highlight the importance of route of administration and cancer type to materials-based targeting, we generated modified versions of several of the figures used by Wilhelm et al. (Figure 4). We emphasize that our present data with PTX-^{14}C-eNPs delivered intraperitoneally (blue circles) or intravenously (red squares) is not contemporaneous with Wilhelm et al.'s data (green diamonds) and is plotted together solely to facilitate comparison with this historical data.

Several observations are noteworthy from the comparison against Wilhelm et al.'s results. First, the vast majority of nanoparticle systems are administered intravenously (114 out of 117, Figure 4A), suggesting that intraperitoneal administration is an under-utilized and under-studied route of administration. Second, selection of active or passive targeting appears to have negligible impact on tumoral delivery and, therefore, alternative strategies should be explored in the future (Figure 4B). Materials-based targeting appears to be a promising strategy, though the present single data point does not guarantee the success of this idea. Additional studies by other researchers will be required in the future. Third, while material composition is essential to materials-based targeting, it offers little differentiation in other targeting contexts (Figure 4C). Fourth, intraperitoneal mesothelioma is an under-studied disease, though this is understandable due to its low incidence rate (Figure 4D). Notwithstanding this, materials-based targeting appears to be ripe for application in other more common peritoneal cancers, such as colon, liver, ovarian, pancreatic, or prostate cancer. In addition to these four analyses, Wilhelm et al. analyzed several other features including material type, shape, hydrodynamic diameter, zeta potential and tumor model, though these do not appear to be differentiating factors (SI Figure 8). Together, these data (Figure 4A−D) demonstrate the synergistic importance of the route of delivery, material design, tumor selection and targeting strategy to achieving significant tumoral delivery of a nanoparticle system.

Clinical relevance of materials-based targeting. While the difference between intravenous and intraperitoneal delivery is stark, it is, perhaps, not surprising that by leveraging the compartmentalization of the body, delivery improves.

https://doi.org/10.1021/acsnano.2c08451
ACS Nano XXXX, XXX, XXX−XXX

Certainly, this has been a motivating strategy for the clinical development of multiple chemotherapy regimens. In one instance, the clinical success of treatments for leukemias may be attributed, in part, to the fact that intravenous administration provides direct access to the target cells within the "compartment" of the circulatory system. In another instance, and directly related to the current study, intraperitoneally administered chemotherapy regimens called "HIPEC" (i.e., Hyperthermic IntraPEritoneal Chemotherapy) result in superior efficacy compared intravenous delivery in ovarian cancer and intraperitoneal mesothelioma.[26,41,42] In fact, intraperitoneal delivery of Taxol results in a 10-fold increase in drug accumulation in mesothelioma tumors compared to intravenous administration.[12,43] Yet, this is 300-fold less improvement than that observed when comparing intravenous and intraperitoneal administration of eNPs (i.e., a 10-fold vs a 3,000-fold increase in tumoral delivery). In this regard, the improvement in tumoral delivery observed in the current study is unexpected and suggests potential clinical utility. For more direct indications of clinical relevance, we turn to previously published studies that demonstrate eNP efficacy in multiple models of mesothelioma. For example, intraperitoneally administered PTX-eNPs result in 10- to 100-fold higher tumoral concentrations of paclitaxel than are achieved with equivalent doses of intraperitoneal Taxol.[12] Furthermore, equivalent doses of intraperitoneally administered PTX-eNPs significantly improve survival compared to equivalent doses of either PTX-loaded PLGA-NPs or Taxol when administered once per week for 4 weeks (72 days vs 43 days and 46 days, respectively).[12,16] Even greater differences in survival are observed with prolonged dosing regimens over 8 weeks (median survival of PTX-eNPs vs Taxol, 103 days vs 49 days, respectively). Together, the present success of "localized" clinical treatment regimens combined with the current preclinical data present a compelling case for the possibility of still greater improvements by leveraging the combination of nanotechnology with the natural compartmentalization of the body.

CONCLUSION

We synthesized a paclitaxel loaded, radiolabeled expansile nanoparticle, the PTX-^{14}C-eNP, and quantified the kinetics of biodistribution following both intravenous and intraperitoneal injection in tumor bearing mice. The quantitative radiolabeling approach used in the current study allowed interrogation of three important questions that were previously unaddressable with fluorescent-only methods, including: 1) what percent of the injected dose reaches and remains in the tumor; 2) what are the primary off-target sites of accumulation; and, 3) what is the quantitative difference between intraperitoneal and intravenous delivery? The results showed that PTX-^{14}C-eNPs localize rapidly and specifically to mesothelioma tumors (e.g., 65% of the injected dose after 6 h) following intraperitoneal injection due to materials-based targeting. In contrast, delivery of the PTX-^{14}C-eNPs via the intravenous route leads to accumulation within the reticuloendothelial system and minimal tumoral accumulation (i.e., <2% of the injected dose after 24 h) as is observed with many other nanoparticle systems. Altogether, the 3,000-fold difference in delivery efficiency between intraperitoneal and intravenous administration is a compelling result that highlights the need for alternative approaches to nanoparticle delivery. Specifically, these results lay a foundation for targeting intraperitoneal tumors and encourages efforts to explore alternative, non-intravenous, routes of delivery to accelerate translation of nanoparticle therapies to the clinic.

METHODS

Quantification of eNP and PLGA-NP Retention within MSTO-211H Cells In Vitro. Rhodamine-labeled eNPs (Rho-eNPs) and rhodamine-labeled PLGA-NPs (Rho-PLGA-NPs) were synthesized according to previously published procedures with equivalent molar ratios of rhodamine.[12] Flow cytometry was used to quantify the retention of Rho-eNPs and Rho-PLGA-NPs in MSTO-211H human mesothelioma tumor cells. Cells were seeded in 6-well plates at 150,000 cells/well in media and allowed to adhere and grow for 24 h. Media was replaced with 2 mL of media containing 25 μg/mL Rho-NPs or Rho-PLGA-NPs (polymer concentration), and cells were incubated for a further 24 h. At this time, particle containing media was removed, the cells were washed thrice with PBS, and fresh media was replaced. Then, following a further 0 h, 24 or 48 h, media was removed, cells were washed thrice with PBS, and fixed in 4% formaldehyde prior to analysis using a BD LSRFortessa flow cytometer (BD Biosciences). Data were analyzed using FlowJo Software.

Synthesis of "hot" 1,1,1-Tris(hydroxymethyl)ethane (SI Figure 9). First, 2.58 g (2.4 mL, 28.4 mmol, 3.3 equiv) of 37% ^{14}C-labeled formaldehyde and 2.5 mL of water were mixed in a 25 mL round-bottomed flask. To this mixture were added slowly 0.5 g (0.62 mL, 8.6 mmol, 1 equiv) of propionaldehyde and a slurry containing 0.43 g (7.8 mmol, 0.9 equiv) of lime (CaO) and 2.5 mL of water (this slurry is prepared 30 min in advance and cooled to room temperature before addition). The glass vial (containing the CaO slurry) was rinsed with 2.5 mL of water (twice) and added to the reaction mixture. The temperature was kept at 30 °C throughout the addition with the aid of cold water when required. Two minutes were required for addition of propionaldehyde, and 10 min for the addition of the lime slurry. After all of the lime slurry was added, the reaction was continued at 30 °C overnight. At the conclusion of this time, the reaction mixture was transferred to a centrifuge tube (extra water was used to transfer all of the reaction mixture). The reaction mixture for 5−10 min (total volume of the mixture was 16 mL). The supernatant was transferred to a round-bottom. Three mL of water were added to the solid, mixed, centrifuged and the supernatant liquid collected and combined with the previous supernatant (total volume = 16 mL + 3 mL = 19 mL). The pH of this solution was around 10 (pH strip). The solution was brought to a pH of 7 by the addition of formic acid (it required only few drops of formic acid) and concentrated at 35 °C under rotary evaporation (making the volume half of the initial volume and taking approximately an hour and a half). This step was performed to remove volatile matter. The solution was lyophilized to obtain a white powder. This white powder contains the final product as well as salt. The product was extracted with 3 × 25 mL MeOH (centrifuge and collect supernatant). The solution was not transparent at this time. After extraction, MeOH was removed via rotary evaporation. The product was dissolved in 25 mL MeOH and filtered through 0.45 μm syringe driven filter. The solution became transparent (clear like water). The solvent was removed via rotary evaporation. The product was then dissolved in 1.5−2 mL of MeOH and precipitated in 120 mL of DCM (drop by drop addition of MeOH into DCM with constant stirring). The white powder was filtered, washed with DCM, drained completely and dried under high vacuum immediately. The product, "hot" 1,1,1-tris(hydroxymethyl)-ethane, was obtained as a white powder: 655 mg (63.3% yield with respect to propionaldehyde; 34% yield with respect to formaldehyde).

Synthesis of "hot" (5-Methyl-2-(2,4,6-trimethoxyphenyl)-1,3-dioxan-5-yl) Methanol (SI Figure 10). First, 1 g (8.3 mmol, 1.1 equiv) of "hot" 1,1,1-tris(hydroxymethyl)ethane, and 1.48 g (7.5 mmol, 1.0 equiv) of 2,4,6-trimethoxybenzaldehyde was dissolved in 50 mL of dry THF in a 100 mL round-bottomed flask. To this mixture, ~2 g of activated molecular sieves type 3A was added as a desiccant. Then, 0.158 g (0.83 mmol, 0.1 equiv) of *p*-toluene sulfonic

https://doi.org/10.1021/acsnano.2c08451
ACS Nano XXXX, XXX, XXX−XXX

acid (monohydrate) (pTSA monohydrate) was added and the reaction was stirred vigorously under N_2 for 4 h. Upon addition of the pTSA monohydrate, a red tint may appear and, after completions of the reaction, a white precipitate is formed and the red color is gone. The THF was removed via rotary evaporation followed by the addition of DCM (29 mL) water (14.5 mL) and saturated $NaHCO_3$ (2.9 mL). The solution was stirred for 15 min and decanted to remove the molecular sieves; the flask/molecular sieves were washed with an additional 2−5 mL of DCM and this combined with the main solution. Note: due to the pH-labile characteristic of the product, from this point forward it is essential that the material not be exposed to acidic conditions; if this occurs, degradation of the product is marked by the appearance of a red tint to the solution. Appropriate precautions are detailed in the following methods. The DCM layer (yellow in color) was separated and isolated from the aqueous layer using a 150 mL separatory funnel and collecting the DCM in a 100 mL round-bottomed flask. The DCM (wet with water and therefore hazy) was dried with the addition of anhydrous sodium sulfate (∼2 g sodium sulfate/10 mL of solution) which resulted in a translucent yellow solution. The sodium sulfate was removed via filtration and, subsequently, the DCM was removed via rotary evaporation. The product was dried on a HiVac for 3−5 h yielding a white or white/blue powder: 78% yield.

Synthesis of "hot" (5-Methyl-2-(2,4,6-trimethoxyphenyl)-1,3-dioxan-5-yl)methyl Methacrylate, i.e., "^{14}C-eNP Monomer" (SI Figure 11). First, 1.12 mL (8.1 mmol; 1.5 equiv) of triethylamine (Et_3N) was added to 30 mL of DCM in a 100 mL round-bottomed flask, to ensure neutral conditions. Then, 1.59 g (5.3 mmol, 1.0 equiv) of "hot" (5-methyl-2-(2,4,6-trimethoxyphenyl)-1,3-dioxan-5-yl) methanol was dissolved in the reaction mixture, and the flask was placed under N_2. It was cooled in an ice bath for 10 min. Next, 0.625 mL (5.4 mmol, 1.2 equiv) of methacryloyl chloride was then added to the reaction mixture dropwise over 2 min. An additional 5 mL of DCM was used to wash down the walls of the flask if splashing occurred. The reaction was stirred overnight under N_2 and allowed to come to room temperature. To the reaction mixture (now a bright yellow liquid) was added 5 mL of saturated $NaHCO_3$ and 5 mL of deionized water. The solution was then stirred for 30 min. This quenches any remaining acid. The DCM layer (yellow in color) was separated and isolated from the aqueous layer using a 150 mL separatory funnel and collecting the DCM in a 100 mL round-bottomed flask. The DCM was dried with the addition of anhydrous sodium sulfate (∼2 g sodium sulfate/10 mL of solution) which resulted in a translucent yellow solution. The sodium sulfate was removed via filtration and, subsequently, the DCM was added to a 100 mL round-bottomed flask and concentrated to ∼5 mL via rotary evaporation. Note: if the crude product is frozen at this point, it may precipitate out as a solid and require the addition of 1−2 mL of DCM (neutralized with triethylamine) to resolubilize it. The product was isolated using silica gel column chromatography (70% yield) as follows: Column: diameter 1"; height: 8" (∼100 mL dry silica) when packed with air; 7.5" when packed tightly (by knocking/jostling the column repeatedly for 3−5 min to help settle the silica; this improves product separation). Dry loading: 1 mL of triethylamine was added to the ∼5 mL of viscous crude product/DCM solution followed by ∼1−2 g of silica (triethylamine neutralizes the acidity of the silica and must therefore be added first to the DCM solution). This was concentrated via rotary evaporation to a viscous slurry. The viscous slurry was then pipetted gently onto the top of the column. If the solution is too viscous, a small amount (1−2 mL) of 9:1 ethyl acetate: triethylamine may be added to help with transfer onto the column. An additional 1−2 mL may be used to wash the round-bottom clean. After loading, ∼0.5" of sand is added to preserve the smooth silica surface. Solvents: The column is packed with 80:10:10 of hexanes: ethyl acetate: triethylamine. A stock of 300 mL should suffice to make the column and provide some solvent to run post loading. After loading the column, run 150 mL of 80:10:10 (hexanes: ethyl acetate: triethylamine) through the column taking it near dry. Run 100 mL of 77:20:3 (hexanes: ethyl acetate: triethylamine) through the column taking it near dry. Start collecting 20 mL fractions. Run 300 mL of 72:25:3 (hexanes:ethyl acetate:triethylamine) through the column. The product was collected in fractions 8−19:70% yield. The product has an R_f value of 0.355 when run in 80:10:10 of hexanes:ethyl acetate:triethylamine on a silica gel aluminum backed TLC plate. Following purification, the ^{14}C-eNP monomer structure was confirmed using an AV400 NMR spectrometer and compared to the cold monomer.

HPLC Analysis of ^{14}C-eNP Monomer Purity. The eNP ^{14}C-eNP monomer was evaluated for purity on a Zorbax SB-Phenyl 3.5 μm 150 × 4.6 mm column at RT using a water (A)/acetonitrile (B) gradient of T(min)/%B 0/40, 20/100, 25/100, 26/40, 30/40 with a flow rate of 1 mL/min and detection at 254 nm.

Mass Spectrometry Analysis of ^{14}C-eNP Monomer. The ^{14}C-eNP monomer structure was confirmed via mass spectrometry and the specific activity found to be 5 mCi/mmol.

Synthesis of "hot" ^{14}C-eNP Polymer (SI Figure 12). First, 1.0 g (2.7 mmol; 1.0 equiv) of ^{14}C-eNP monomer was added to a 10 mL round-bottomed flask. Note: If this reaction is performed on a 0.5 g scale, the volume of anisole should be reduced to 2 mL. Then, 2.24 mg (0.0135 mmol; 0.005 equiv) of AIBN was added to the round-bottomed flask via a freshly created stock solution of 1 mg AIBN/mL anisole (i.e., 2.24 mL of this solution were used). The anisole was previously dried for 4 h over activated molecular sieves Type 3A. An additional 2.76 mL of anisole was added to the reaction vessel to bring the total volume to 5 mL. The reaction vessel was sealed against the air, and 3 freeze−pump−thaw cycles (see below) were used to degas the solution (note, a stir bar must be added before this process is begun). Freeze−Pump−Thaw: i. put the vessel under N_2 atmosphere; ii. freeze in liquid N_2; iii. put under HIVAC vacuum for ∼3 min; iv. return to N_2 atmosphere; v. thaw in warm water; vi. repeat steps i.−v. two more times. The reaction was then stirred under N_2 and placed in an oil bath. The oil bath was heated to 70 °C and the reaction allowed to run overnight for 16 h. The reaction was removed from the oil bath and allowed to cool to room temperature. The solution is viscous (e.g., honey) and may have a yellow tint; there may even be some cloudy white precipitate. If the solution is too viscous to easily pipette (or precipitate is visible), a small quantity (2−3 mL) of DCM may be added to thin the solution. The solution was then precipitated dropwise into ice cold methanol (50 mL) that was being vigorously stirred. After the product was precipitated, it was allowed to stir for an additional 10 min. The product was collected via filtration and dried under HIVAC for 4−6 h to yield a white flaky solid: >80% yield on 1 g scale; 60% yield on 0.5 g scale. The polymer molecular weight was determined via gel permeation chromatography (GPC), see below. Note: The HIVAC pump was an Edwards Vacuum RV8 115/230 V, 1-ph, 50/60 Hz. Following purification, the ^{14}C-eNP polymer structure was confirmed using an AV400 NMR spectrometer with the ^{14}C-eNP polymer dissolved in $CDCl_3$.

GPC Analysis of ^{14}C-eNP Polymer Molecular Weight (MW). The polymer was analyzed on a Waters Styragel HR 5E DMF 300 × 7.8 mm column at RT using DMF containing 0.05 mol LiBr with a flow rate of 0.5 mL/min. The injection volume was 50 μL.

GPC Analysis of ^{14}C-eNP Polymer Stability. The polymer was reanalyzed at 2 weeks and 4 weeks following synthesis to evaluate whether scission or cross-linking of the polymer, due to the radioisotopes, occurred.

Nanoparticle Synthesis. Nanoparticle synthesis followed previously published pprotocols.[15] In brief, 147 mg of the ^{14}C-eNP polymer and 53 mg of the cold eNP polymer were combined with 10 mg of paclitaxel in 2 mL of DCM, and this mixture was sonicated with 8 mL of 12 mg/mL sodium dodecyl sulfate in a 50 mM phosphpate buffer prior to postprocessing via LV1 (process pressure 15,000 psi) for form PTX-^{14}C-eNPs.

Biodistribution of ^{14}C-eNPs in Tumor Bearing Animals. For this study, we employed the same intraperitoneal tumor model as previously published.[12,16] However, as tumor models, growth rates and survival times are known to vary when performed in different laboratories, we first performed a pilot model development study to ensure the successful transfer of the model to inviCRO. Eight nude mice were xenografted with 5 × 10^6 MSTO-211H mesothelioma

https://doi.org/10.1021/acsnano.2c08451
ACS Nano XXXX, XXX, XXX−XXX

tumor cells in the peritoneum. Two animals each were then sacrificed 7, 14, 21 and 28 days post xenografting, and the gross tumor burden was evaluated. At week 2, tumors were present in both animals with tumor mass ranging from 5 to 27 mg. At week 4, both animals had too many tumors to be collected and were near moribund. Therefore, to balance the need to have established tumors with the need to ensure the survival of the animals to a 2 week time point post particle injection, 14 days post xenografting was selected as the time of particle injection.

Using this model and timing scheme, animals in the main cohort were injected intraperitoneally with 250 μL of ^{14}C-eNPs (8.63 μCi) and sacrificed 2 h, 6 h, 24 h, 7 days and 14 days following injection. At each time point, the primary organs and tissues were harvested, digested and the radioactivity measured via liquid scintillation counting (LSC) (N = 3/time point). A second cohort of animals received intravenous injections of ^{14}C-eNPs via the tail vein with identical processing (N = 3/time point). These animals were sacrificed at 2 h, 24 h and 7 days post nanoparticle injection.

ASSOCIATED CONTENT

Supporting Information

The Supporting Information is available free of charge at https://pubs.acs.org/doi/10.1021/acsnano.2c08451.

NMR and mass spectral analysis of ^{14}C-eNP Monomer (SI Figure 1); HPLC analysis of ^{14}C-eNP monomer (SI Figure 2); NMR and GPC analysis of radiochemical purity of ^{14}C-eNP polymer (SI Figures 3 and 4); standard curve of ^{14}C-eNP radioactivity (SI Figure 5); alternative representation of main text Figure 2 with y-axes scaled individually for each plot rather than uniformly across all plots (SI Figure 6); histopathological sections of animal lung, liver and spleen (SI Figure 7); additional subpanels from Wilhelm et al.'s original publication, including material type, shape, hydrodynamic diameter, zeta potential and tumor model (SI Figure 8); synthesis schematic and NMR of ^{14}C-eNP monomer and precursors as well as (SI Figures 9−11) ^{14}C-eNP polymer (SI Figure 12) (PDF)

AUTHOR INFORMATION

Corresponding Author

Aaron H. Colby − *Boston University, Boston, Massachusetts 02215, United States; Ionic Pharmaceuticals, LLC, Watertown, Massachusetts 02472, United States;* orcid.org/0000-0001-7161-821X; Email: acolby@bu.edu

Authors

Jack Kirsch − *Boston University, Boston, Massachusetts 02215, United States*

Amit N. Patwa − *Boston University, Boston, Massachusetts 02215, United States; Navrachana University, Vadodara 391410, India*

Rong Liu − *Massachusetts General Hospital, Boston, Massachusetts 02114, United States*

Beth Hollister − *HighRock Consulting, Oxford, North Carolina 27565, United States*

William McCulloch − *Alba BioPharm Advisors, Inc., Raleigh, North Carolina 27614, United States*

Joanna E. Burdette − *University of Illinois at Chicago, Chicago, Illinois 60607, United States;* orcid.org/0000-0002-7271-6847

Cedric J. Pearce − *Mycosynthetix, Inc., Hillsborough, North Carolina 27278, United States*

Nicholas H. Oberliels − *Ionic Pharmaceuticals, LLC, Watertown, Massachusetts 02472, United States; University of North Carolina at Greensboro, Greensboro, North Carolina 27412, United States;* orcid.org/0000-0002-0354-8464

Yolonda L. Colson − *Massachusetts General Hospital, Boston, Massachusetts 02114, United States*

Kebin Liu − *Augusta University, Augusta, Georgia 30912, United States;* orcid.org/0000-0003-1965-7240

Mark W. Grinstaff − *Boston University, Boston, Massachusetts 02215, United States; Ionic Pharmaceuticals, LLC, Watertown, Massachusetts 02472, United States;* orcid.org/0000-0002-5453-3668

Complete contact information is available at: https://pubs.acs.org/10.1021/acsnano.2c08451

Funding

The authors thank the following generous funding sources: National Cancer Institute, including: R43 CA189215, R43 CA213538, R44 CA189215, R01 CA227433 and R01 CA232056; National Institute of Biomedical Imaging and Bioengineering, including: T32 EB006359.

Notes

The authors declare the following competing financial interest(s): A.H.C., N.H.O. and M.W.G. have ownership interest in Ionic Pharmaceuticals, LLC. B.A.H. and W.M. serve as consultants to Ionic Pharmaceuticals.

REFERENCES

(1) Armstrong, D. K.; Fleming, G. F.; Markman, M.; Bailey, H. H. A Phase I Trial of Intraperitoneal Sustained-Release Paclitaxel Microspheres (Paclimer®) in Recurrent Ovarian Cancer: A Gynecologic Oncology Group Study. *Gynecol. Oncol.* **2006**, *103*, 391−396.

(2) Zhao, J.; Koay, E. J.; Li, T.; Wen, X.; Li, C. A Hindsight Reflection on the Clinical Studies of Poly(L-Glutamic Acid)-Paclitaxel. *Wiley Interdiscip. Rev. Nanomed. Nanobiotechnol.* **2018**, *10*, No. e1497.

(3) Maeda, H.; Nakamura, H.; Fang, J. The EPR Effect for Macromolecular Drug Delivery to Solid Tumors: Improvement of Tumor Uptake, Lowering of Systemic Toxicity, and Distinct Tumor Imaging in Vivo. *Adv. Drug Delivery Rev.* **2013**, *65*, 71−79.

(4) Prabhakar, U.; Maeda, H.; Jain, R. K.; Sevick-Muraca, E. M.; Zamboni, W.; Farokhzad, O. C.; Barry, S. T.; Gabizon, A.; Grodzinski, P.; Blakey, D. C. Challenges and Key Considerations of the Enhanced Permeability and Retention Effect for Nanomedicine Drug Delivery in Oncology. *Cancer Res.* **2013**, *73*, 2412−2417.

(5) Goldberg, M. S.; Hook, S. S.; Wang, A. Z.; Bulte, J. W.; Patri, A. K.; Uckun, F. M.; Cryns, V. L.; Hanes, J.; Akin, D.; Hall, J. B.; Gharkholo, N.; Mumper, R. J. Biotargeted Nanomedicines for Cancer: Six Tenets before You Begin. *Nanomedicine (Lond)* **2013**, *8*, 299−308.

(6) Tyner, K.; Sadrieh, N. Considerations When Submitting Nanotherapeutics to FDA/CDER for Regulatory Review. *Methods Mol. Biol.* **2011**, *697*, 17−31.

(7) Groenendijk, F. H.; Bernards, R. Drug Resistance to Targeted Therapies: Déjà Vu All Over Again. *Mol. Oncol.* **2014**, *8*, 1067−1083.

(8) Holohan, C.; Van Schaeybroeck, S.; Longley, D. B.; Johnston, P. G. Cancer Drug Resistance: An Evolving Paradigm. *Nat. Rev. Cancer* **2013**, *13*, 714−726.

(9) Wilhelm, S.; Tavares, A. J.; Dai, Q.; Ohta, S.; Audet, J.; Dvorak, H. F.; Chan, W. C. W. Analysis of Nanoparticle Delivery to Tumours. *Nat. Rev. Materials* **2016**, *1*, 1−12.

(10) Colby, A. H.; Liu, R.; Schulz, M. D.; Padera, R. F.; Colson, Y. L.; Grinstaff, M. W. Two-Step Delivery: Exploiting the Partition Coefficient Concept to Increase Intratumoral Paclitaxel Concentrations in Vivo Using Responsive Nanoparticles. *Sci. Rep.* **2016**, *6*, 1−10.

(11) Herrera, V. L.; Colby, A. H.; Tan, G. A.; Moran, A. M.; O'Brien, M. J.; Colson, Y. L.; Ruiz-Opazo, N.; Grinstaff, M. W. Evaluation of Expansile Nanoparticle Tumor Localization and Efficacy in a Cancer Stem Cell-Derived Model of Pancreatic Peritoneal Carcinomatosis. *Nanomedicine (Lond)* **2016**, *11*, 1001−1015.
(12) Liu, R.; Colby, A. H.; Gilmore, D.; Schulz, M.; Zeng, J.; Padera, R. F.; Shirihai, O.; Grinstaff, M. W.; Colson, Y. L. Nanoparticle Tumor Localization, Disruption of Autophagosomal Trafficking, and Prolonged Drug Delivery Improve Survival in Peritoneal Mesothelioma. *Biomaterials* **2016**, *102*, 175−186.
(13) Colby, A. H.; Berry, S. M.; Moran, A. M.; Pasion, K. A.; Liu, R.; Colson, Y. L.; Ruiz-Opazo, N.; Grinstaff, M. W.; Herrera, V. L. Highly Specific and Sensitive Fluorescent Nanoprobes for Image-Guided Resection of Sub-Millimeter Peritoneal Tumors. *ACS Nano* **2017**, *11*, 1466−1477.
(14) Chu, N. Q.; Liu, R.; Colby, A.; de Forcrand, C.; Padera, R. F.; Grinstaff, M. W.; Colson, Y. L. Paclitaxel-Loaded Expansile Nanoparticles Improve Survival Following Cytoreductive Surgery in Pleural Mesothelioma Xenografts. *J. Thorac. Cardiovasc. Surg.* **2020**, *160*, e159−e168.
(15) Colby, A. H.; Liu, R.; Doyle, R. P.; Merting, A.; Zhang, H.; Savage, N.; Chu, N. Q.; Hollister, B. A.; McCulloch, W.; Burdette, J. E.; Pearce, C. J.; Liu, K.; Oberlies, N. H.; Colson, Y. L.; Grinstaff, M. W. Pilot-Scale Production of Expansile Nanoparticles: Practical Methods for Clinical Scale-Up. *J. Controlled Release* **2021**, *337*, 144−154.
(16) Colby, A. H.; Oberlies, N. H.; Pearce, C. J.; Herrera, V. L.; Colson, Y. L.; Grinstaff, M. W. Nanoparticle Drug-Delivery Systems for Peritoneal Cancers: A Case Study of the Design, Characterization and Development of the Expansile Nanoparticle. *Wiley Interdiscip. Rev. Nanomed. Nanobiotechnol.* **2017**, *9*, 1−20.
(17) Hanahan, D.; Weinberg, R. A. The Hallmarks of Cancer. *Cell* **2000**, *100*, 57−70.
(18) Hanahan, D.; Weinberg, R. A. Hallmarks of Cancer: The Next Generation. *Cell* **2011**, *144*, 646−674.
(19) Gilmore, D.; Schulz, M.; Liu, R.; Zubris, K. A.; Padera, R. F.; Catalano, P. J.; Grinstaff, M. W.; Colson, Y. L. Cytoreductive Surgery and Intraoperative Administration of Paclitaxel-Loaded Expansile Nanoparticles Delay Tumor Recurrence in Ovarian Carcinoma. *Ann. Surg. Oncol.* **2013**, *20*, 1684−1693.
(20) Salvi, A.; Amrine, C. S. M.; Austin, J. R.; Kilpatrick, K.; Russo, A.; Lantvit, D.; Calderon-Gierszal, E.; Mattes, Z.; Pearce, C. J.; Grinstaff, M. W.; Colby, A. H.; Oberlies, N. H.; Burdette, J. E. Verticillin a Causes Apoptosis and Reduces Tumor Burden in High-Grade Serous Ovarian Cancer by Inducing DNA Damage. *Mol. Cancer Ther.* **2020**, *19*, 89−100.
(21) Colson, Y. L.; Liu, R.; Southard, E. B.; Schulz, M. D.; Wade, J. E.; Griset, A. P.; Zubris, K. A.; Padera, R. F.; Grinstaff, M. W. The Performance of Expansile Nanoparticles in a Murine Model of Peritoneal Carcinomatosis. *Biomaterials* **2011**, *32*, 832−840.
(22) Schulz, M. D.; Zubris, K. A.; Wade, J. E.; Padera, R. F.; Xu, X.; Grinstaff, M. W.; Colson, Y. L. Paclitaxel-Loaded Expansile Nanoparticles in a Multimodal Treatment Model of Malignant Mesothelioma. *Ann. Thorac. Surg.* **2011**, *92*, 2007−2013.
(23) Markman, M. Clinical Efficacy Supporting the Role of Intraperitoneal Drug Delivery in the Primary Chemotherapeutic Management of Small-Volume Residual Advanced Ovarian Cancer. *Semin. Oncol.* **2006**, *33*, 3−7.
(24) Fujiwara, K.; Markman, M.; Morgan, M.; Coleman, R. L. Intraperitoneal Carboplatin-Based Chemotherapy for Epithelial Ovarian Cancer. *Gynecol. Oncol.* **2005**, *97*, 10−15.
(25) Wright, A. A.; Cronin, A.; Milne, D. E.; Bookman, M. A.; Burger, R. A.; Cohn, D. E.; Cristea, M. C.; Griggs, J. J.; Keating, N. L.; Levenback, C. F.; Mantia-Smaldone, G.; Matulonis, U. A.; Meyer, L. A.; Niland, J. C.; Weeks, J. C.; O'Malley, D. M. Use and Effectiveness of Intraperitoneal Chemotherapy for Treatment of Ovarian Cancer. *J. Clin. Oncol.* **2015**, *33*, 2841−2847.
(26) Armstrong, D. K.; Bundy, B.; Wenzel, L.; Huang, H. Q.; Baergen, R.; Lele, S.; Copeland, L. J.; Walker, J. L.; Burger, R. A. Intraperitoneal Cisplatin and Paclitaxel in Ovarian Cancer. *N. Engl. J. Med.* **2006**, *354*, 34−43.
(27) Monk, B. J.; Chan, J. K. Is Intraperitoneal Chemotherapy Still an Acceptable Option in Primary Adjuvant Chemotherapy for Advanced Ovarian Cancer? *Ann. Oncol.* **2017**, *28*, viii40−viii45.
(28) Holmberg, S. B.; Forssell-Aronsson, E.; Gretarsdottir, J.; Jacobsson, L.; Rippe, B. Vascular Clearance by the Reticuloendothelial System–Measurements Using Two Different-Sized Albumin Colloids. *Scand. J. Clin. Lab. Invest.* **1990**, *50*, 865−871.
(29) Wagner, H. N., Jr.; Iio, M. Studies of the Reticuloendothelial System (RES). 3. Blockade of the RES in Man. *J. Clin. Invest.* **1964**, *43*, 1525−1532.
(30) Zubris, K. A. V.; Liu, R.; Colby, A.; Schulz, M. D.; Colson, Y. L.; Grinstaff, M. W. In Vitro Activity of Paclitaxel-Loaded Polymeric Expansile Nanoparticles in Breast Cancer Cells. *Biomacromolecules* **2013**, *14*, 2074−2082.
(31) Karran, S. J.; Leach, K. G.; Wisbey, M. L.; Blumgart, L. H. Uptake of a Colloid in Rat Liver Following Intravenous Intrasplenic and Intramesenteric Injection. *J. Nucl. Med.* **1975**, *16*, 377−379.
(32) Ilium, L.; Davis, S. S.; Wilson, C. G.; Thomas, N. W.; Frier, M.; Hardy, J. G. Blood Clearance and Organ Deposition of Intravenously-Administered Colloidal Particles the Effects of Particle Size, Nature and Shape. *Int. J. Pharm.* **1982**, *12*, 135−146.
(33) Rejman, J.; Oberle, V.; Zuhorn, I. S.; Hoekstra, D. Size-Dependent Internalization of Particles Via the Pathways of Clathrin- and Caveolae-Mediated Endocytosis. *Biochem. J.* **2004**, *377*, 159−169.
(34) Owens, D. E., III; Peppas, N. A. Opsonization, Biodistribution, and Pharmacokinetics of Polymeric Nanoparticles. *Int. J. Pharm.* **2006**, *307*, 93−102.
(35) Storm, G.; Belliot, S. O.; Daemen, T.; Lasic, D. D. Surface Modification of Nanoparticles to Oppose Uptake by the Mononuclear Phagocyte System. *Adv. Drug Delivery Rev.* **1995**, *17*, 31−48.
(36) Alexis, F.; Pridgen, E.; Molnar, L. K.; Farokhzad, O. C. Factors Affecting the Clearance and Biodistribution of Polymeric Nanoparticles. *Mol. Pharmaceutics* **2008**, *5*, 505−515.
(37) Cheng, Y.-H.; He, C.; Riviere, J. E.; Monteiro-Riviere, N. A.; Lin, Z. Meta-Analysis of Nanoparticle Delivery to Tumors Using a Physiologically Based Pharmacokinetic Modeling and Simulation Approach. *ACS Nano* **2020**, *14*, 3075−3095.
(38) Varani, M.; Campagna, G.; Bentivoglio, V.; Serafinelli, M.; Martini, M. L.; Galli, F.; Signore, A. Synthesis and Biodistribution of ^{99m}Tc-Labeled Plga Nanoparticles by Microfluidic Technique. *Pharmaceutics* **2021**, *13*, 1769−1782.
(39) Farrag, N. S.; El-Sabagh, H. A.; Al-mahallawi, A. M.; Amin, A. M.; AbdEl-Bary, A.; Mamdouh, W. Comparative Study on Radiolabeling and Biodistribution of Core-Shell Silver/Polymeric Nanoparticles-Based Theranostics for Tumor Targeting. *Int. J. Pharm.* **2017**, *529*, 123−133.
(40) Wang, H.; Guo, P. Radiolabeled Rna Nanoparticles for Highly Specific Targeting and Efficient Tumor Accumulation with Favorable in Vivo Biodistribution. *Mol. Pharmaceutics* **2021**, *18*, 2924−2934.
(41) Sugarbaker, P. H.; Stuart, O. A. Pharmacokinetics of the Intraperitoneal Nanoparticle Pegylated Liposomal Doxorubicin in Patients with Peritoneal Metastases. *Eur. J. Surg. Oncol.* **2021**, *47*, 108−114.
(42) Mohamed, F.; Marchettini, P.; Stuart, O. A.; Sugarbaker, P. H. Pharmacokinetics and Tissue Distribution of Intraperitoneal Paclitaxel with Different Carrier Solutions. *Cancer Chemother. Pharmacol* **2003**, *52*, 405−410.
(43) Sabatelle, R. C.; Liu, R.; Hung, Y. P.; Bressler, E.; Neal, E. J.; Martin, A.; Ekladious, I.; Grinstaff, M. W.; Colson, Y. L. Ultra-High Drug Loading Improves Nanoparticle Efficacy against Peritoneal Mesothelioma. *Biomaterials* **2022**, *285*, 121534.

https://doi.org/10.1021/acsnano.2c08451
ACS Nano XXXX, XXX, XXX−XXX